JACS
JOURNAL OF THE AMERICAN CHEMICAL SOCIETY

Communication

pubs.acs.org/JACS

Crystalline Carbon Nitride Nanosheets for Improved Visible-Light Hydrogen Evolution

Katharina Schwinghammer,[†,‡] Maria B. Mesch,[∥] Viola Duppel,[†] Christian Ziegler,[‡,†,§] Jürgen Senker,[∥] and Bettina V. Lotsch*[,†,‡,§]

[†]Max Planck Institute for Solid State Research, 70569 Stuttgart, Germany

[‡]Department of Chemistry, University of Munich, LMU, 81377 Munich, Germany

[§]Nanosystems Initiative Munich (NIM) and Center for Nanoscience, 80799 Munich, Germany

[∥]Inorganic Chemistry III, University of Bayreuth, 95447 Bayreuth, Germany

Supporting Information

ABSTRACT: Nanosheets of a crystalline 2D carbon nitride were obtained by ionothermal synthesis of the layered bulk material poly(triazine imide), PTI, followed by one-step liquid exfoliation in water. Triazine-based nanosheets are 1-2 nm in height and afford chemically and colloidally stable suspensions under both basic and acidic conditions. We use solid-state NMR spectroscopy of isotopically enriched, restacked nanosheets as a tool to indirectly monitor the exfoliation process and carve out the chemical changes occurring upon exfoliation, as well as to determine the nanosheet thickness. PTI nanosheets show significantly enhanced visible-light driven photocatalytic activity toward hydrogen evolution compared to their bulk counterpart, which highlights the crucial role of morphology and surface area on the photocatalytic performance of carbon nitride materials.

The exploration of highly efficient photocatalysts has been fuelled by the prospect of converting sustainable solar energy into clean chemical fuels.[1] In this context, carbon nitrides have emerged as promising metal-free visible-light photocatalysts owing to their abundance, stability, and chemical tunability.[2] Recently, we[3] and others[4] independently discovered a new type of carbon nitride photocatalyst, poly(triazine imide) (PTI/Li^+Cl^-),[5a,b] which rivals the benchmark carbon nitride based on heptazine building blocks, known as melon[6] and often loosely called graphitic carbon nitride, *g*-C_3N_4.[2,7] In contrast to melon ("*g*-C_3N_4"), PTI is a crystalline species and represents the only structurally characterized two-dimensional (2D) carbon nitride network known to date.[5] The layers are composed of imide-linked triazine units (Figure 1a) and are stacked in an ABA-type fashion, separated by weak van der Waals forces, with lithium and chloride ions situated in channels running along the stacking direction (Figure 1b).[5b] In the past, various strategies, such as doping with heteroatoms[8] or organic molecules,[3,9] interfacing with other semiconductors or dyes to create heterojunctions,[10] and morphology-tuning[8c,11] have been used to increase the photocatalytic activity of carbon nitrides. In this regard, the exfoliation of carbon nitrides into ultrathin nanosheets has been shown to enhance the photocatalytic activity due to surface and quantum confinement effects.[12] Since the seminal discovery of graphene,[13] it has been well-established that delamination of 2D layered materials such as MoS_2[14] and WS_2[15] may entail unique physicochemical properties, including ultrahigh charge carrier mobilities and pronounced changes in the band structure. Likewise, delamination of layered photocatalysts into 2D sheets may be advantageous for promoting photocatalytic efficiency, both via the exposure of active sites and optimized light harvesting, charge separation and percolation.[12a−c,16] In contrast to melon-type carbon nitrides which have been exfoliated recently,[12a] PTI is highly crystalline and a true 2D material,[5b,12d] which lends itself as an excellent model system to explore both structural effects and photocatalytic activity as a function of the exfoliation state.

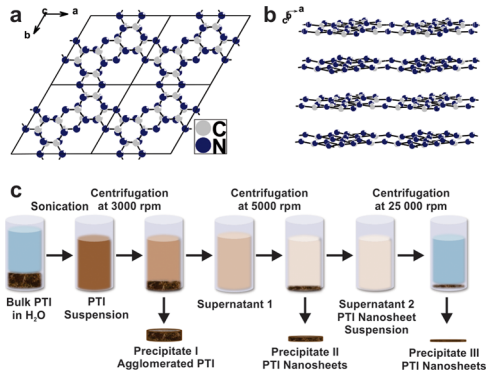

Figure 1. Idealized PTI structure (lithium/chloride intercalation omitted for clarity) viewed along the *c*-axis (a) and the slightly tilted *b*-axis (b). Scheme of the exfoliation process and product labeling (c).

Layered materials such as graphite and boron nitride can be exfoliated when the enthalpy of mixing is minimized, which is the case when the surface energies of the nanosheet and solvent match.[17] Zhang et al.[12b] calculated the surface energy of *g*-C_3N_4 as 115 mJ/m^2, which matches well with the surface energy of water (~102 mJ/m^2).[17c] In addition, the terminal hydrogen atoms of the carbon nitrides prefer polar solvents, which upon hydrogen bond formation will cause swelling and exfoliation of the bulk carbon nitrides on a large scale.[12b] Recently, Bojdys et al.

Received: November 6, 2013
Published: January 16, 2014

   dx.doi.org/10.1021/ja411321s | *J. Am. Chem. Soc.* 2014, 136, 1730−1733

reported[12d] that bromide intercalated PTI can be exfoliated by intercalation of potassium and subjecting the intercalate to water. The resulting thin sheets show large lateral sizes in the micrometer range, which however is expected to be unfavorable for photocatalysis due to the relatively small surface area and exposed number of active sites.

Here we demonstrate the one-step synthesis of crystalline PTI nanosheets by "green" liquid phase exfoliation in water, without the need for additives, toxic solvents or preintercalation steps. Remarkably, facile exfoliation in water leads to highly crystalline nanosheets of 1-2 nm in thickness, which show significantly increased photocatalytic efficiency for visible-light driven hydrogen evolution compared to bulk crystalline PTI.

Crystalline PTI/Li^+Cl^- was suspended in water (2 mg/mL) and sonicated for 15 h at room temperature (Figure 1c). The dispersion was centrifuged at 3000 rpm to remove aggregates (Precipitate I), giving rise to a homogeneous dispersion of PTI nanosheets. To further separate the suspension according to the degree of exfoliation, a fraction of the aqueous suspension was further centrifuged at 5000 rpm (Precipitate II) to yield a nanosheet suspension with a higher degree of exfoliation compared to Precipitate I. The supernatant remaining after this centrifugation step, showing the maximum degree of exfoliation, was kept for analysis of the suspended nanosheets (Supernatant 2, 0.2 mg/mL). Finally, the nanosheets were precipitated by centrifugation at 25000 rpm and subjected to analysis in order to compare the suspended nanosheets (Supernatant 2) vs their restacked form (Precipitate III). The labeling scheme of the different nanosheet fractions is outlined in Figure 1c.

The well-dispersed PTI nanosheets (Supernatant 2) in water are negatively charged, with a zeta potential of −54.0 mV and a pH of 10.5. This observation is consistent with the fact that deprotonated, bridging imide moieties are present which are charge-compensated by Li ions, giving rise to dynamic lithium-proton exchange with water and, hence, to the observed basic character of the suspension caused by lithium hydroxide. The brownish dispersion is highly stable, showing no signs of precipitation even after being stored for 2 months, in line with the high negative surface charge. Interestingly, the surface charge is minimal (point of zero charge) at pH 5.4 and reversed at lower pH with a zeta potential of +30 mV at pH 2 (Figure S1). Thus, the nanosheets are stable both at low (<3) and high pH values (>8), which can be rationalized by the overall amphoteric character of the ring and bridging nitrogen functions in the PTI backbone.

Having ascertained the state of dispersion and stability of the suspensions, the thickness of as-prepared PTI nanosheets (Supernatant 2) was investigated by atomic force microscopy (AFM). According to Wirnhier et al. bulk PTI is built up from hollow microtubes whose walls are composed of an oriented assembly of hexagonal prismatic crystallites with lateral sizes of about 60 nm.[5b] AFM images of the nanosheet suspension (Supernatant 2) and the corresponding height profile display exfoliated crystallites with lateral sizes of less than 100 nm and a height of 1-2 nm, indicating the exfoliated nanosheets are composed of only a few carbon nitride layers, taking into account a water shell likely surrounding the nanosheets (Figure 2a and discussion below).

AFM results were further confirmed by TEM investigations. HRTEM measurements reveal that the hexagonal shape of the crystallites is in fact retained, and the 2D sheets are well-separated and conformally spread across the substrate (Figure 2c). Selected area electron diffraction (SAED) patterns are fully

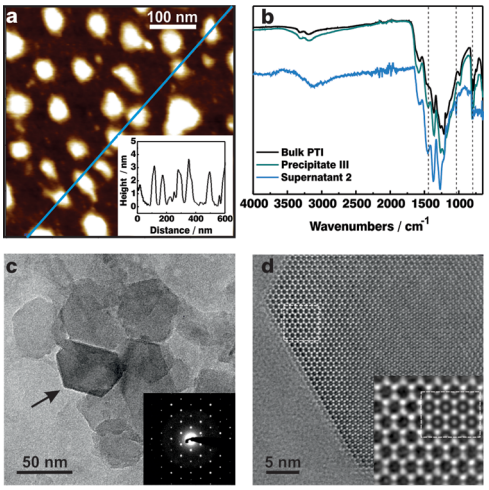

Figure 2. AFM image of exfoliated PTI nanosheets deposited on a Si/SiO_2 wafer (a) and the corresponding height image (inset). IR spectrum of bulk PTI (black) compared to Precipitate III (green) and Supernatant 2 (blue) (b). TEM image of exfoliated ultrathin PTI nanosheets (c), higher magnification of a PTI nanosheet edge viewed along [001] (d) marked in (c) and simulation (JEMS; Δf = +50 nm, t = 2.70 nm; inset).

consistent with the expected hexagonal symmetry of an individual PTI layer (Figures 2c (inset) and S2a).[5b]

X-ray diffraction patterns (Figure S2b) confirm that both the restacked PTI nanosheets (Precipitate III) and the precipitates from the previous steps (Precipitate I and II) show reflections which are consistent with bulk PTI,[5a,b] confirming that the structure of the parent bulk PTI is retained in the nanosheets. Interestingly, the presence of (*hkl*) reflections showing no obvious asymmetry or line broadening further suggests that the same stacking pattern is adopted after centrifugation, without the occurrence of turbostratic disorder in the restacked material.

The identity of the nanosheets was further confirmed by FTIR spectroscopy (Figure 2b). The characteristic IR spectrum of the nanosheet Precipitate II is largely reminiscent of that of the bulk material,[5a,b] both having a band at 810 cm^{-1} (triazine ring sextant out of plane bending) and a fingerprint region 1200-1620 cm^{-1} which is dominated by the same ν(C-NH-C) and ν(C═N) stretching vibrations. Nevertheless, Precipitate II shows a more highly resolved band at 1440 cm^{-1} and the intensity ratio of the ν(C-NH-C) vibrations at 1260 and 1210 cm^{-1} is slightly shifted. The IR of the nanosheet suspension (Supernatant 2, measured in solution against a water background) shows slightly broadened and shifted bands in the region between 1000 and 1200 cm^{-1} compared to the bulk material. These changes can be attributed to the water environment of the nanosheets in Supernatant 2.

The composition of the nanosheets (Precipitate III) was analyzed by elemental analysis (EA), revealing slight differences from the bulk material (Table S1). PTI nanosheets show a decreased lithium content compared to the starting material, suggesting that lithium ions are released during the exfoliation process, possibly by Li^+-H^+ exchange at the strongly basic bridging imide groups through reaction with water. The atomic C/N ratio of Precipitate II (0.62) is similar to the one in bulk PTI (0.64).

To further probe the chemical environment and bonding between the carbon and nitrogen atoms in the PTI nanosheets (Precipitate III), XPS measurements were conducted. No obvious shifts of the binding energy of C 1s and N 1s core electrons are observable, suggesting that the chemical states of

dx.doi.org/10.1021/ja411321s | J. Am. Chem. Soc. 2014, 136, 1730−1733

both carbon and nitrogen atoms in the nanosheets (Precipitate III) are the same as in bulk PTI (Supporting Information (SI)). Two oxygen peaks are observed for Precipitate III, which are due to air (O1 at 530.8 eV) and water (532.1 eV), respectively (Figure S4).[18] Note that the bulk material contains only the first oxygen peak (O1).

To gain more insights into the local structure of the nanosheets relative to the one of bulk PTI, we performed solid-state NMR spectroscopy with ^{15}N isotope-enriched samples of Precipitates I–III and bulk PTI in comparison (Figure 3). While being overall similar, both ^{13}C and ^{15}N spectra

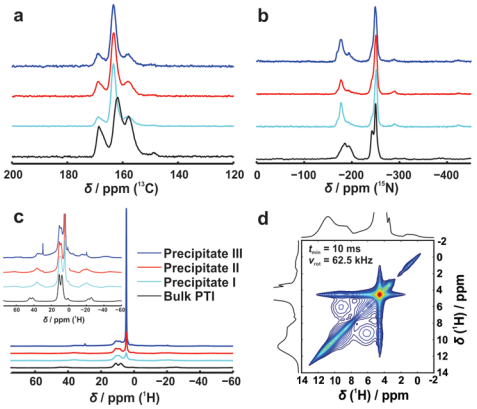

Figure 3. ^{13}C (a) and ^{15}N (b) CP–MAS NMR spectra and ^{1}H (c) MAS NMR spectra for Precipitates I-III and bulk PTI, respectively. $^{1}H^{1}H$ proton driven spin diffusion spectrum (d) for Precipitate III.

reveal subtle differences in the relative signal intensities on going from the bulk to the restacked nanosheets. These changes are predominantly attributed to a decrease in the lithium content in the channels and the resulting higher local symmetry of carbon and nitrogen environments in the restacked samples. As the Li content does not further decrease with increasing degree of exfoliation, it is likely determined initially by the sonication process and unaffected by the subsequent centrifugation-exfoliation steps. In contrast, the water content in the samples, apparent from ^{1}H spectra (signals at 6.2 and 4.6 ppm), tremendously increases from Precipitate I to III. Polarization exchange between the PTI protons and the ones of the water molecules as ascertained by $^{1}H^{1}H$ proton driven spin diffusion spectroscopy (Figures 3d and S6) is even faster than the exchange among the PTI protons. This points to a close vicinity of the nanosheets and water on a molecular scale. Assuming dense monolayers of water on the surface of the nanosheet stacks, we find that between 2 and 4 PTI layers are interspersed with two water layers, based on the relative proton signal intensities (SI and Figure S5). The derived height of the nanosheet stack $(PTI)_{2\text{-}4}$ corresponds well to that measured by AFM (1-2 nm). Therefore, NMR presents a viable "bulk method" to indirectly determine the thickness of nanosheet stacks.

The brown color of the PTI nanosheet suspension indicates substantial absorption in the visible range of the spectrum, similar to bulk PTI. While the strong absorption edge just below 400 nm is likewise present in the nanosheet suspension, the broad band around 450 nm is less pronounced for Supernatant 2 (measured in water), which may be due to the absence of layer stacking or to solvation effects. Quantum confinement effects are not noticeable, since there are only minute changes in the absorption properties for the precipitates (Figure S7) and nanosheet suspension (Figure 4d), respectively, compared to the bulk

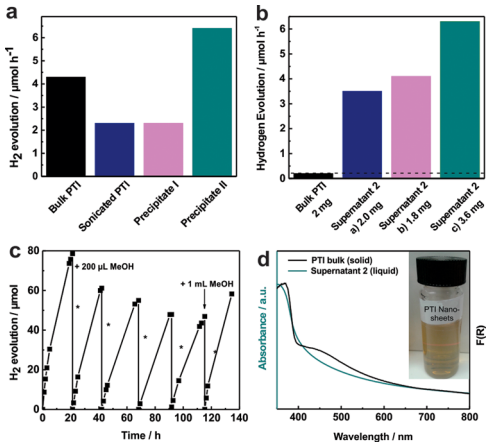

Figure 4. Photocatalytic activity toward H_2 production of the Pt-doped Precipitates (I and II) compared to sonicated PTI and bulk PTI (a), and of the nanosheet suspensions compared to bulk PTI (b), measured in a 10 vol% TEoA/water solution for 3 h illumination with visible light (>420 nm). Cyclic stability tests of the nanosheet suspension: Supernatant 1 with methanol as electron donor (c). The reactor was purged several times (marked with an asterisk) and methanol was reinjected twice. UV/vis spectrum of bulk PTI measured as solid in diffuse reflectance mode compared to Supernatant 2 measured as liquid in transmission mode (d).

material. More insights into the electronic band structure is given by Moewes and co-workers, who extracted a band gap of 2.2 eV for the LiCl-intercalated material.[20]

Owing to their small particle size and, thus, higher exposed surface area and possibly higher number of active sites, the PTI nanosheets were tested for photocatalytic hydrogen evolution and compared to the water reduction activity of the bulk material. The photocatalytic activity of the PTI nanosheet suspension (Supernatant 2), of the bulk material as well as agglomerated PTI (Precipitate I) and partially exfoliated nanosheet fractions (Precipitate II) was measured in a water/triethanolamine (TEoA) solution (for details see SI) under visible light illumination (Figure 4a). Under the conditions applied, bulk PTI evolves 4.3 μmol H_2/h. Sonication of the material for 15 h in water lowers the activity of the suspension by about 43%. The formed agglomerates were centrifuged at 3000 rpm, redispersed and tested with regard to their photocatalytic activity, confirming the same low activity of Precipitate I compared to sonicated PTI. Precipitate II, containing partially exfoliated PTI, shows an improvement in hydrogen evolution by 28% (6.4 μmol H_2/h).

To examine the low concentrated PTI nanosheet suspensions (Supernatant 2), 2 mg of bulk PTI was tested and compared to three different suspensions (2a, 2b and 2c) containing 2.0, 1.8, and 3.6 mg of nanosheets, respectively. While bulk PTI shows an activity of 0.2 μmol H_2/h (Figure 4b), 2 mg of the PTI nanosheets (Supernatant 2a) exhibits a much higher hydrogen evolution rate, corresponding to an improvement by a factor of 18 (3.5 μmol H_2/h; 1.3% apparent quantum efficiency at 400 nm for nonoptimized conditions, see ref 21) as compared to the bulk material. As expected, the more concentrated nanosheet suspension (Supernatant 2c) shows an even higher photocatalytic activity, suggesting that hydrogen evolution is not yet diffusion limited under these conditions and light harvesting is not yet impeded by scattering effects.

dx.doi.org/10.1021/ja411321s | J. Am. Chem. Soc. 2014, 136, 1730–1733

Measurements probing whether sustained hydrogen evolution over extended periods of time is feasible were performed with Supernatant 1 and TEoA (Figure S8) or methanol as electron donor (Figure 4c). While with TEoA a decrease in activity was detected, which may be due to degradation of the material under basic conditions, long-term measurements in methanol show that the PTI nanosheets are steadily evolving hydrogen for at least 130 h. Note that after the sixth cycle (after addition of methanol), the hydrogen evolution rate of the first cycle (6.1 μmol H_2/h) could almost be recovered (5.4 μmol H_2/h). Furthermore, a strongly wavelength-dependent hydrogen evolution rate was observed (Figure S9).

In conclusion, triazine-based PTI nanosheets have been successfully synthesized through a simple and cost-effective aqueous exfoliation method starting with bulk PTI powder. The structure and morphology of the nanosheets was identified by complementary techniques including TEM, XRD, AFM and solid-state NMR spectroscopy, highlighting the close relationship between the parent PTI and the nanosheets. In agreement with AFM measurements revealing nanosheet thicknesses of 1-2 nm, NMR points to facile water incorporation in the restacked nanosheets, forming arrangements of 2-4 PTI layers interspersed with water layers. Exfoliated PTI is the first structurally well-defined, crystalline 2D carbon nitride showing high activity toward photocatalytic water-splitting, which is among the highest ever observed for pristine carbon nitrides, including mesoporous "*g*-C_3N_4".[9a,12a,19] The photocatalytic activity of the exfoliated sample is superior by a factor of >17 to both the nonexfoliated counterpart and melon (internal standard) and by a factor of >8 to "*g*-C_3N_4" (calculated for 2 mg).[12a]

Our study draws on highly defined, structurally unambiguous carbon nitride nanosheets and thus paves the way for a better understanding of structure-property relationships in carbon nitrides and the factors influencing the photocatalytic activity in this promising, yet still largely ill-defined, class of photocatalysts.

■ ASSOCIATED CONTENT

Supporting Information

Experimental details and characterization data. This material is available free of charge via the Internet at http://pubs.acs.org.

■ AUTHOR INFORMATION

Corresponding Author

b.lotsch@fkf.mpg.de

Notes

The authors declare no competing financial interest.

■ ACKNOWLEDGMENTS

Financial support by the Deutsche Forschungsgemeinschaft (projects LO1801/1-1, SE1417/5-1), the cluster of excellence "Nanosystems Initiative Munich" (NIM), and the Center for NanoScience (CeNS) is gratefully acknowledged. We thank M. Konuma and M.-L. Schreiber for their assistance with the sample characterization and N. Popp for the synthesis of ^{15}N-enriched PTI. Dedicated to Professor Ingo-Peter Lorenz on the Occasion of His 70th Birthday.

■ REFERENCES

(1) (a) Hoffmann, M. R.; Scot, T. M.; Choi, W.; Bahnemann, D. W. *Chem. Rev.* **1995**, *95*, 69. (b) Linsebigler, A. L.; Lu, G.; Yates, J. T. *Chem. Rev.* **1995**, *95*, 735.

(2) (a) Wang, X.; Maeda, K.; Thomas, A.; Takanabe, K.; Xin, G.; Carlsson, J. M.; Domen, K.; Antonietti, M. *Nat. Mater.* **2009**, *8*, 76. (b) Wang, Y.; Wang, X.; Antonietti, M. *Angew. Chem., Int. Ed.* **2012**, *51*, 68. (c) Zheng, Y.; Liu, J.; Liang, J.; Jaroniec, M.; Qiao, S. Z. *Energy Environ. Sci.* **2012**, *5*, 6717.

(3) Schwinghammer, K.; Tuffy, B.; Mesch, M. B.; Wirnhier, E.; Martineau, C.; Taulelle, F.; Schnick, W.; Senker, J.; Lotsch, B. V. *Angew. Chem., Int. Ed.* **2013**, *52*, 2435.

(4) Ham, Y.; Maeda, K.; Cha, D.; Takanabe, K.; Domen, K. *Chem.—Asian J.* **2013**, *8*, 218.

(5) (a) Bojdys, M. J.; Müller, J.-O.; Antonietti, M.; Thomas, A. *Chem.—Eur. J.* **2008**, *14*, 8177. (b) Wirnhier, E.; Döblinger, M.; Gunzelmann, D.; Senker, J.; Lotsch, B. V.; Schnick, W. *Chem.—Eur. J.* **2011**, *17*, 3213. (c) Chong, S. Y.; Jones, J. T. A.; Khimyak, Y. Z.; Cooper, A. I.; Thomas, A.; Antonietti, M.; Bojdys, M. J. *J. Mater. Chem. A* **2013**, *1*, 1102.

(6) Lotsch, B. V.; Döblinger, M.; Sehnert, J.; Seyfarth, L.; Senker, J.; Oeckler, O.; Schnick, W. *Chem.—Eur. J.* **2007**, *13*, 4969.

(7) (a) Yu, J.; Wang, S.; Cheng, B.; Lin, Z.; Huang, F. *Catal. Sci. Technol.* **2013**, *3*, 1782. (b) Liao, G.; Chen, S.; Quan, X.; Yu, H.; Zhao, H. *J. Mater. Chem.* **2012**, *22*, 2721. (c) Bai, X.; Wang, L.; Zong, R.; Zhu, Y. *J. Phys. Chem. C* **2013**, *117*, 9952.

(8) (a) Wang, Y.; Zhang, J.; Wang, X.; Antonietti, M.; Li, H. *Angew. Chem., Int. Ed.* **2010**, *49*, 3356. (b) Liu, G.; Niu, P.; Sun, C.; Smith, S. C.; Chen, Z.; Lu, G. Q.; Cheng, H.-M. *J. Am. Chem. Soc.* **2010**, *132*, 11642. (c) Lin, Z.; Wang, X. *Angew. Chem., Int. Ed.* **2013**, *52*, 1735.

(9) (a) Zhang, J. H.; Chen, X. F.; Takanabe, K.; Maeda, K.; Domen, K.; Epping, J. D.; Fu, X. Z.; Antonietti, M.; Wang, X. C. *Angew. Chem., Int. Ed.* **2010**, *122*, 451. (b) Zhang, J.; Zhang, G.; Chen, X.; Lin, S.; Möhlmann, L.; Dołęga, G.; Lipner, G.; Antonietti, M.; Blechert, S.; Wang, X. *Angew. Chem., Int. Ed.* **2012**, *51*, 3183.

(10) (a) Wang, Y.; Shi, R.; Lin, J.; Zhu, Y. *Energy Environ. Sci.* **2011**, *4*, 2922. (b) Zhang, Y.; Mori, T.; Ye, J.; Antonietti, M. *J. Am. Chem. Soc.* **2010**, *132*, 6294.

(11) (a) Kiskan, B.; Zhang, J.; Wang, X.; Antonietti, M.; Yagci, Y. *ACS Macro Lett.* **2012**, *1*, 546. (b) Wang, X.; Maeda, K.; Chen, X.; Takanabe, K.; Domen, K.; Hou, Y.; Fu, X.; Antonietti, M. *J. Am. Chem. Soc.* **2009**, *131*, 1680.

(12) (a) Yang, S.; Gong, Y.; Zhang, J.; Zhan, L.; Ma, L.; Fang, Z.; Vajtai, R.; Wang, X.; Ajayan, P. M. *Adv. Mater.* **2013**, *25*, 2452. (b) Zhang, X.; Xie, X.; Wang, H.; Zhang, J.; Pan, B.; Xie, Y. *J. Am. Chem. Soc.* **2013**, *135*, 18. (c) Niu, P.; Zhang, L.; Liu, G.; Cheng, H.-M. *Adv. Funct. Mater.* **2012**, *22*, 4763. (d) Bojdys, M. J.; Severin, N.; Rabe, J. P.; Cooper, A. I.; Thomas, A.; Antonietti, M. *Macromol. Rapid Commun.* **2013**, *34*, 850.

(13) (a) Cai, M.; Thorpe, D.; Adamson, D. H.; Schniepp, H. C. *J. Mater. Chem.* **2012**, *22*, 24992. (b) Geim, A. K.; Novoselov, K. S. *Nat. Mater.* **2007**, *6*, 183.

(14) Štengl, V.; Henych, J. *Nanoscale* **2013**, *5*, 3387.

(15) Voiry, D.; Yamaguchi, H.; Li, J.; Silva, R.; Alves, D. C. B.; Fujita, T.; Chen, M.; Asefa, T.; Shenoy, V. B.; Eda, G.; Chhowalla, M. *Nat. Mater.* **2013**, *12*, 850.

(16) (a) Ebina, Y.; Sakai, N.; Sasaki, T. *J. Phys. Chem. B* **2005**, *109*, 17212. (b) Ida, S.; Okamoto, Y.; Koga, S.; Hagiwara, H.; Ishihara, T. *RSC Adv.* **2013**, *3*, 11521. (c) Wang, W.; Yu, J. C.; Xia, D.; Wong, P. K.; Li, Y. *Environ. Sci. Technol.* **2013**, *47*, 8724.

(17) (a) Coleman, J. N.; Lotya, M.; ÓNeill, A.; Bergin, S. D.; King, P. J.; Khan, U.; Young, K.; Gaucher, A.; De, S.; Smith, R. J.; et al. *Science* **2011**, *331*, 568. (b) Bergin, S. D.; Nicolosi, V.; Streich, P. V.; Giordani, S.; Sun, Z.; Windle, A. H.; Ryan, P.; Niraj, N. P. P; Wang, Z.-T. T.; Carpenter, L.; et al. *Adv. Mater.* **2008**, *20*, 1876. (c) Since the surface tension of water equals 72.1 mJ/m^2, the surface energy of the nanosheet suspension (~102 mJ/m^2) can be calculated considering the temperature and the entropy factor.[17a,b]

(18) George, G. A. *Polym. Int.* **1994**, *33*, 439.

(19) Chen, X.; Jun, Y.-S.; Takanabe, K.; Maeda, K.; Domen, K.; Fu, X.; Antonietti, M.; Wang, X. *Chem. Mater.* **2009**, *21*, 4093.

(20) McDermott, E. J.; Wirnhier, E.; Schnick, W.; Virdi, K. S.; Scheu, C.; Kauffmann, Y.; Kaplan, W. D.; Kurmaev, E. Z.; Moewes, A. *J. Phys. Chem. C* **2013**, *117*, 8806.

(21) Ohtani, B. *J. Photochem. Photobiol., C* **2010**, *11*, 157.